A Wavelet-GSM Approach to Demosaicking

Jiachao Zhang, *Student Member, IEEE*, Andong Sheng, and Keigo Hirakawa, *Senior Member, IEEE*

***Abstract*—We propose a wavelet-based Gaussian scale mixture (GSM) demosaicking method. The wavelet coefficients of the proposed method corresponding to the luminance and chrominance components are reconstructed using Bayesian minimum mean square error estimation. The proposed wavelet-GSM prior exploits the correlation of neighboring wavelets coefficients to improve upon a previously proposed posterior sparsity directed demosaicking method. As a result, our proposed demosaicking method suppresses the zippering artifacts more effectively than the state of the arts.**

***Index Terms*—Demosaicking, Gaussian scale mixture (GSM).**

I. Introduction

A COLOR image is typically captured by Bayer color filter array (CFA), a spatial multiplexing of color filters of red, green, and blue filters, as shown in Fig. 1(a) [1]. The task of reconstructing a full color image from CFA-sampled data is called demosaicking or CFA interpolation. Demosaicking plays a crucial role in recovering high-quality images and has been studied extensively[2]–[4]. Yet, standard benchmarking datasets are comprised of 0.375-megapixel color images obtained from scanned film images [5], [6], where image resolution is much smaller than that of the real raw sensor data and is treated with gamma correction. Thus, the reported benchmarking performances are poor predictors for actual demosaicking performance on real raw sensor data. In fact, it is not uncommon for the "best performing" demosaicking methods to suffer from demosaicking artifacts when tested on actual sensor data. (see Fig. 3) This fact underscores the need for continuing progress in demosaicking research.

In this letter, we propose to modify the posterior sparsity-directed demosaicking (PSDD) method [7] by replacing the sparsity assumption in PSDD by a Gaussian scale mixture (GSM) [8]. The wavelet coefficients corresponding to the luminance and chrominance components are reconstructed using Bayesian minimum-mean-square-error (MMSE) estimation. As a result of exploiting the correlation of neighboring wavelet coefficients, we significantly improve on the PSDD results. When tested on real sensor data, the proposed algorithm achieves higher image quality than that of the state-of-the-art demosaicking methods, even though the benchmarking results on standard image set are inferior.

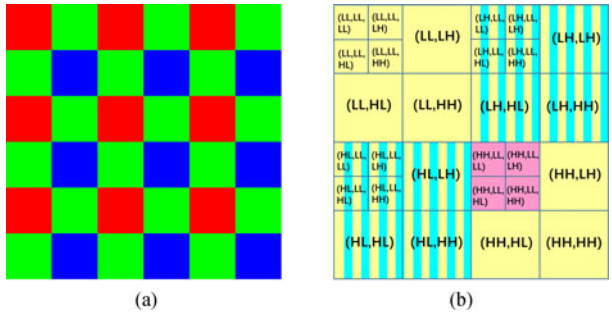

(a) (b)

Fig. 1. (a) Bayer CFA and (b) Mallat wavelet transform. For (b), sub-bands are indexed as $\boldsymbol{i} = (i_1, i_2, ..., i_J)$, where i_j denotes the orientation of the jth-level decomposition. The supports of $U_{\boldsymbol{n}}^{\boldsymbol{i}}$ and the sub-band-modulate $V_{\boldsymbol{n}}^{\boldsymbol{i}}$ and $W_{\boldsymbol{n}}^{\boldsymbol{i}}$ in $S_{\boldsymbol{n}}^{\boldsymbol{i}}$ are represented by yellow, cyan, and magenta, respectively. ($\kappa = 2\,J = 3$ in this case.)

II. Background and Related Works

A. Background: Demosaicking Algorithms

The image sensor value $Y_{\boldsymbol{n}}$ at pixel location $\boldsymbol{n} = (n_x, n_y)$ is

$$Y_{\boldsymbol{n}} = \boldsymbol{C}_{\boldsymbol{n}} \boldsymbol{X}_{\boldsymbol{n}} \tag{1}$$

where $\boldsymbol{X}_{\boldsymbol{n}} = (X_{\boldsymbol{n}}^1, X_{\boldsymbol{n}}^2, X_{\boldsymbol{n}}^3)^T$ represents the "complete" color image in sensor color space, and $\boldsymbol{C}_{\boldsymbol{n}}$ is the filter indicator function ($\boldsymbol{C}_{\boldsymbol{n}} = (1, 0, 0)$ for red pixel, for instance). The goal of demosaicking is to recover $\boldsymbol{X}_{\boldsymbol{n}}$ from the sensor value $Y_{\boldsymbol{n}}$.

Modern demosaicking methods exploit the spatial correlation between the color components to avoid color artifacts at object boundaries. Motivated by the assumption that the quotient of two color channels is slowly varying, the method in [9] reconstructs the missing color components by smoothing the red-green and blue–green ratios. Alternatively, many interpolation algorithms [10]–[12] and CFA patterns [13] leverage the band-limitedness of the differences between the color components. Recent algorithms [5], [14]–[16] exploit the fact that residual images are even smoother than the color differences.

A heuristic wavelet analysis of the CFA-sampled images yielded lossless raw sensor data compression method in [17]. A more rigorous analysis of wavelet/filterbank sampling theory in [18] gave rise to the wavelet-based demosaicking method in

Manuscript received December 7, 2017; revised March 10, 2018; accepted March 20, 2018. Date of publication April 4, 2018; date of current version April 26, 2018. This work was supported in part by the National Natural Science Foundation of China under Grant 61702265, in part by the Natural Science Foundation of Jiangsu Province under Grant BK20170856, and in part by the CCF-Tencent Open Research Fund (PI: Xiangbo Shu). The associate editor coordinating the review of this manuscript and approving it for publication was Dr. Vasileios Mezaris. *(Corresponding author: Jiachao Zhang.)*

J. Zhang is with the Kangni Mechanical and Electrical Institute, Nanjing Institute of Technology, Nanjing 211167, China, and also with the Department of Automation, Nanjing University of Science and Technology, Nanjing 210094, China (e-mail: zhangjc07@foxmail.com).

A. Sheng is with the Department of Automation, Nanjing University of Science and Technology, Nanjing 210094, China (e-mail: shengandong@mail.njust.edu.cn).

K. Hirakawa is with the Department of Electrical and Computer Engineering, University of Dayton, Dayton OH 45469 USA (e-mail: khirakawa1@udayton.edu).

This paper has supplementary downloadable material available at http://ieeexplore.ieee.org..

Color versions of one or more of the figures in this paper are available online at http://ieeexplore.ieee.org.

Digital Object Identifier 10.1109/LSP.2018.2822802

[11] and the PSDD method in [7] improved the demosaicking performance. In this letter, we propose to soften the sparsity assumption in PSDD using GSM (see Section III) to improve demosaicking performance further. GSM has the additional benefit that the correlation of the neighboring wavelet coefficients can be exploited.

B. Review: PSDD

Let $\boldsymbol{C_n}$ be a Bayer CFA pattern. Define $\boldsymbol{M} \in \mathbb{R}^{3\times 3}$ as

$$\boldsymbol{M} = \begin{bmatrix} 1/4 & 1/2 & 1/4 \\ 1/4 & 0 & -1/4 \\ 1/4 & -1/2 & 1/4 \end{bmatrix}. \tag{2}$$

We rewrite (1) as

$$Y_{\boldsymbol{n}} = \boldsymbol{C_n X_n} = \boldsymbol{C_n M^{-1} M X_n} = \boldsymbol{C}'_{\boldsymbol{n}} \boldsymbol{X}'_{\boldsymbol{n}} \tag{3}$$

where

$$\boldsymbol{C}'_{\boldsymbol{n}} = \boldsymbol{C_n M^{-1}} = \begin{bmatrix} 1 & (-1)^{n_x} + (-1)^{n_y} & (-1)^{n_x+n_y} \end{bmatrix} \tag{4}$$

$$\boldsymbol{X}'_{\boldsymbol{n}} = \boldsymbol{M X_n} = \begin{bmatrix} (X^1_{\boldsymbol{n}} + 2X^2_{\boldsymbol{n}} + X^3_{\boldsymbol{n}})/4 \\ (X^1_{\boldsymbol{n}} - X^3_{\boldsymbol{n}})/4 \\ (X^1_{\boldsymbol{n}} - 2X^2_{\boldsymbol{n}} + X^3_{\boldsymbol{n}})/4 \end{bmatrix}. \tag{5}$$

In the demosaicking literature, we treat $X'^1_{\boldsymbol{n}}$ as a proxy for luminance image, and $X'^2_{\boldsymbol{n}}$ and $X'^3_{\boldsymbol{n}}$ as proxies for chrominance components [19]–[21]. Thanks to the nonsingularity of matrix $\boldsymbol{M}$, the demosaicking task of estimating $\boldsymbol{X_n}$ from $Y_{\boldsymbol{n}}$ is equivalent to reconstructing $\boldsymbol{X}'_{\boldsymbol{n}}$ from $Y_{\boldsymbol{n}}$.

Let $S^{\boldsymbol{i}}_{\boldsymbol{n}}$ and $[U^{\boldsymbol{i}}_{\boldsymbol{n}}, V^{\boldsymbol{i}}_{\boldsymbol{n}}, W^{\boldsymbol{i}}_{\boldsymbol{n}}]^T$ denote the J-level Mallat wavelet transform [see Fig. 1(b)] coefficients of $Y_{\boldsymbol{n}}$ and $\boldsymbol{X}'_{\boldsymbol{n}}$ in (3), respectively. Here, $\boldsymbol{i} = (i_1, i_2, ..., i_J)$ is the sub-band index, where $i_j \in \{\text{LL,LH,HL,HH}\}$ indicates the separable orientation of the jth level decomposition. For example, $S^{(\text{LL,LH})}_{\boldsymbol{n}}$ is the second-level wavelet coefficient computed by applying one-level wavelet transform to $S^{\text{LL}}_{\boldsymbol{n}}$ and keeping the LH sub-band [7], [18], etc.

The Haar wavelet analysis in [18], proved the following:

$$\begin{aligned} S^{(\text{LL},\boldsymbol{i}')}_{\boldsymbol{n}} &= U^{(\text{LL},\boldsymbol{i}')}_{\boldsymbol{n}} + V^{(\text{HL},\boldsymbol{i}')}_{\boldsymbol{n}} + V^{(\text{LH},\boldsymbol{i}')}_{\boldsymbol{n}} + W^{(\text{HH},\boldsymbol{i}')}_{\boldsymbol{n}} \\ S^{(\text{LH},\boldsymbol{i}')}_{\boldsymbol{n}} &= U^{(\text{LH},\boldsymbol{i}')}_{\boldsymbol{n}} + V^{(\text{HH},\boldsymbol{i}')}_{\boldsymbol{n}} + V^{(\text{LL},\boldsymbol{i}')}_{\boldsymbol{n}} + W^{(\text{HL},\boldsymbol{i}')}_{\boldsymbol{n}} \\ S^{(\text{HL},\boldsymbol{i}')}_{\boldsymbol{n}} &= U^{(\text{HL},\boldsymbol{i}')}_{\boldsymbol{n}} + V^{(\text{LL},\boldsymbol{i}')}_{\boldsymbol{n}} + V^{(\text{HH},\boldsymbol{i}')}_{\boldsymbol{n}} + W^{(\text{LH},\boldsymbol{i}')}_{\boldsymbol{n}} \\ S^{(\text{HH},\boldsymbol{i}')}_{\boldsymbol{n}} &= U^{(\text{HH},\boldsymbol{i}')}_{\boldsymbol{n}} + V^{(\text{LH},\boldsymbol{i}')}_{\boldsymbol{n}} + V^{(\text{HL},\boldsymbol{i}')}_{\boldsymbol{n}} + W^{(\text{LL},\boldsymbol{i}')}_{\boldsymbol{n}} \end{aligned} \tag{6}$$

where $\boldsymbol{i}' = (i_2, i_3, ..., i_J)$ (if not Haar, see [18]). We assume that the Mallat wavelet packet coefficients are bandlimited

$$\begin{aligned} U^{\boldsymbol{i}}_{\boldsymbol{n}} &= 0 \quad \text{if } i_1 = \text{HH and } J \leqslant \kappa \\ V^{\boldsymbol{i}}_{\boldsymbol{n}} &= 0 \quad \text{if } i_1 \neq \text{LL} \\ W^{\boldsymbol{i}}_{\boldsymbol{n}} &= 0 \quad \text{if } i_1 \neq \text{LL or } J > \kappa \end{aligned} \tag{7}$$

where κ denotes the wavelet-domain bandwidth and J is the total number of wavelet decomposition processed. Equation (6) can be simplified by substituting the assumptions in (7)

$$S^{\boldsymbol{i}}_{\boldsymbol{n}} = \begin{cases} V^{(\text{LL},\boldsymbol{i}')}_{\boldsymbol{n}} + U^{\boldsymbol{i}}_{\boldsymbol{n}} & \text{if } i_1 \in \{\text{LH, HL}\} \\ W^{(\text{LL},\boldsymbol{i}')}_{\boldsymbol{n}} & \text{if } i_1 = \text{HH and } J \leqslant \kappa \\ U^{\boldsymbol{i}}_{\boldsymbol{n}} & \text{else.} \end{cases} \tag{8}$$

We previously proved in [7] that when U is sufficiently sparse, a "hard decision" in PSDD was near-optimal for overcoming the hazards of aliasing [7]

Theorem 1: (Posterior Sparsity) Suppose $U^{\boldsymbol{i}}_{\boldsymbol{n}}$ is θ-sparse

$$P[U^{\boldsymbol{i}}_{\boldsymbol{n}} = 0] = \theta.$$

If the distribution of $U^{\boldsymbol{i}}_{\boldsymbol{n}}$ is symmetric about zero, then

$$\widehat{V}^{(\text{LL},\boldsymbol{i}')}_{\boldsymbol{n}} = \begin{cases} S^{(\text{LH},\boldsymbol{i}')}_{\boldsymbol{n}} & \text{if } |S^{(\text{LH},\boldsymbol{i}')}_{\boldsymbol{n}}| > |S^{(\text{HL},\boldsymbol{i}')}_{\boldsymbol{n}}| \\ S^{(\text{HL},\boldsymbol{i}')}_{\boldsymbol{n}} & \text{else} \end{cases} \tag{9}$$

$$\widehat{U}^{\boldsymbol{i}}_{\boldsymbol{n}} = \begin{cases} S^{\boldsymbol{i}}_{\boldsymbol{n}} - \widehat{V}^{(\text{LL},\boldsymbol{i}')}_{\boldsymbol{n}} & \text{if } i_1 \in \{\text{LH, HL}\} \\ S^{\boldsymbol{i}}_{\boldsymbol{n}} & \text{if } i_1 = \text{LL or } \{i_1 = \text{HH and } J > \kappa\} \end{cases}$$

$$\widehat{W}^{(\text{LL},\boldsymbol{i}')}_{\boldsymbol{n}} = S^{(\text{HH},\boldsymbol{i}')}_{\boldsymbol{n}} \quad \text{for } J \leqslant \kappa$$

is correct with probability greater than θ.

The color image $\widehat{\boldsymbol{X}}_{\boldsymbol{n}}$ is recovered by taking inverse wavelet transform of $\widehat{U}^{\boldsymbol{i}}_{\boldsymbol{n}}$, $\widehat{V}^{\boldsymbol{i}}_{\boldsymbol{n}}$, $\widehat{W}^{\boldsymbol{i}}_{\boldsymbol{n}}$, and inverting $\boldsymbol{M}$.

III. Proposed Demosaicking Algorithm

If θ is close to 1, the method in (9) is almost always correct. PSDD fails if the wavelet coefficients are not sparse enough (i.e., θ not sufficiently large). To improve its performance, we adopt the Bayesian perspective. That is, we explicitly model the prior density for the latent wavelet coefficients using GSM. GSM is not strictly "sparse," but it promotes small reconstructed values while preserving the edges.

A. Prior Model: GSM

One standard way to model the heavy-tailed distribution of the wavelet coefficients is by GSM [8]. Let $\boldsymbol{V}^{(\text{LL},\boldsymbol{i}')}_{\boldsymbol{n}}$ and $\boldsymbol{U}^{\boldsymbol{i}}_{\boldsymbol{n}}$ ($i_1 \in \{\text{LH, HL}\}$) denote the latent sharp coefficients within an $\sqrt{m} \times \sqrt{m}$ spatial neighborhood of $\boldsymbol{n}$ (vectorized to $\mathbb{R}^m$). The random vectors $\boldsymbol{V}^{(\text{LL},\boldsymbol{i}')}_{\boldsymbol{n}}$ and $\boldsymbol{U}^{\boldsymbol{i}}_{\boldsymbol{n}} \in \mathbb{R}^m$ can be defined as a GSM

$$\begin{aligned} &\text{Ø}_{\boldsymbol{n}} | \boldsymbol{z}_{\boldsymbol{n}} \sim \mathcal{N}(0, \boldsymbol{\Sigma}_{\text{Ø}|\boldsymbol{z}}) \\ &\boldsymbol{\Sigma}_{\text{Ø}|\boldsymbol{z}} = \text{diag}([z^{\text{LL}}_{\boldsymbol{n}} \boldsymbol{\Sigma}^{\text{LL}} z^{\text{LH}}_{\boldsymbol{n}} \boldsymbol{\Sigma}^{\text{LH}} z^{\text{HL}}_{\boldsymbol{n}} \boldsymbol{\Sigma}^{\text{HL}}]) \end{aligned} \tag{10}$$

where $\text{Ø}_{\boldsymbol{n}} = [\boldsymbol{V}^{(\text{LL},\boldsymbol{i}')^T}_{\boldsymbol{n}} \boldsymbol{U}^{(\text{LH},\boldsymbol{i}')^T}_{\boldsymbol{n}} \boldsymbol{U}^{(\text{HL},\boldsymbol{i}')^T}_{\boldsymbol{n}}]^T$; and $\boldsymbol{z} = [z^{\text{LL}}\ z^{\text{LH}}\ z^{\text{HL}}]^T \in \mathbb{R}^3$ are the hidden mixture weights; $\boldsymbol{\Sigma}^{\text{LL}}$, $\boldsymbol{\Sigma}^{\text{LH}}$, and $\boldsymbol{\Sigma}^{\text{HL}} \in \mathbb{R}^{m\times m}$ are the covariance matrices of $\boldsymbol{V}^{(\text{LL},\boldsymbol{i}')}_{\boldsymbol{n}}$, $\boldsymbol{U}^{(\text{LH},\boldsymbol{i}')}_{\boldsymbol{n}}$, and $\boldsymbol{U}^{(\text{HL},\boldsymbol{i}')}_{\boldsymbol{n}}$, respectively.

B. Likelihood Function

For the likelihood model, we assume that there is small amount of deviation from (1) due to read-out noise and model error. Consider the observation $Q_{\boldsymbol{n}}$ of the form

$$Q_{\boldsymbol{n}} | Y_{\boldsymbol{n}} \sim \mathcal{N}(Y_{\boldsymbol{n}}, \boldsymbol{\Lambda}_N) \tag{11}$$

where $\mathbf{\Lambda}_N$ is the variance of model error. The corresponding likelihood function of the wavelet coefficient $T_{\boldsymbol{n}}$ of $Q_{\boldsymbol{n}}$ is

$$\begin{bmatrix} T_{\boldsymbol{n}}^{(\mathrm{LH},i')} \\ T_{\boldsymbol{n}}^{(\mathrm{HL},i')} \end{bmatrix} \Bigg| X_{\boldsymbol{n}} \sim \mathcal{N}\left(\begin{bmatrix} V_{\boldsymbol{n}}^{(\mathrm{LL},i')} + U_{\boldsymbol{n}}^{(\mathrm{LH},i')} \\ V_{\boldsymbol{n}}^{(\mathrm{LL},i')} + U_{\boldsymbol{n}}^{(\mathrm{HL},i')} \end{bmatrix}, \begin{bmatrix} \mathbf{\Lambda}_N & 0 \\ 0 & \mathbf{\Lambda}_N \end{bmatrix} \right) \tag{12}$$

$$T_{\boldsymbol{n}}^{\boldsymbol{i}} | X_{\boldsymbol{n}} \sim \begin{cases} \mathcal{N}(U_{\boldsymbol{n}}^{\boldsymbol{i}}, \mathbf{\Lambda}_N) & \text{if } i_1 = \mathrm{LL} \text{ or } \{i_1 = \mathrm{HH} \text{ and } J > \kappa\} \\ \mathcal{N}(W_{\boldsymbol{n}}^{(\mathrm{LL},i')}, \mathbf{\Lambda}_N) & \text{if } i_1 = \mathrm{HH} \text{ and } J \leqslant \kappa \end{cases} \tag{13}$$

where J and κ are as defined in (7). By (10), the marginal density of $T_{\boldsymbol{n}}$ conditioned on $\boldsymbol{z}$ is also a normal

$$\begin{bmatrix} T_{\boldsymbol{n}}^{(\mathrm{LH},i')} \\ T_{\boldsymbol{n}}^{(\mathrm{HL},i')} \end{bmatrix} \Bigg| \boldsymbol{z}_{\boldsymbol{n}} \sim \mathcal{N}\left(\begin{bmatrix} 0 \\ 0 \end{bmatrix} \begin{bmatrix} z_{\boldsymbol{n}}^{\mathrm{LL}} \mathbf{\Sigma}^{\mathrm{LL}} + z_{\boldsymbol{n}}^{\mathrm{LH}} \mathbf{\Sigma}^{\mathrm{LH}} + \mathbf{\Lambda}_N & z_{\boldsymbol{n}}^{\mathrm{LL}} \mathbf{\Sigma}^{\mathrm{LL}} \\ z_{\boldsymbol{n}}^{\mathrm{LL}} \mathbf{\Sigma}^{\mathrm{LL}} & z_{\boldsymbol{n}}^{\mathrm{LL}} \mathbf{\Sigma}^{\mathrm{LL}} + z_{\boldsymbol{n}}^{\mathrm{HL}} \mathbf{\Sigma}^{\mathrm{HL}} + \mathbf{\Lambda}_N \end{bmatrix} \right). \tag{14}$$

C. Wavelet-GSM Demosaicking

Consider reconstructing luminance components $U_{\boldsymbol{n}}^{\boldsymbol{i}}$ ($i_1 \in \{\mathrm{LH}, \mathrm{HL}\}$) and chrominance $V_{\boldsymbol{n}}^{(\mathrm{LL},i')}$ in (10) from wavelet coefficient $T_{\boldsymbol{n}}^{\boldsymbol{i}}$. The MMSE estimate is the posterior mean

$$\begin{aligned} \hat{\mathcal{O}}_{\boldsymbol{n}} &= \mathbb{E}\left[\mathcal{O}_{\boldsymbol{n}} \Bigg| \begin{bmatrix} T_{\boldsymbol{n}}^{(\mathrm{LH},i')} \\ T_{\boldsymbol{n}}^{(\mathrm{HL},i')} \end{bmatrix} \right] \\ &= \int_{\mathbb{R}^3} \mathbb{E}\left[\mathcal{O}_{\boldsymbol{n}} \Bigg| \begin{bmatrix} T_{\boldsymbol{n}}^{(\mathrm{LH},i')} \\ T_{\boldsymbol{n}}^{(\mathrm{HL},i')} \end{bmatrix}, \boldsymbol{z}_{\boldsymbol{n}} \right] p\left(\boldsymbol{z}_{\boldsymbol{n}} \Bigg| \begin{bmatrix} T_{\boldsymbol{n}}^{(\mathrm{LH},i')} \\ T_{\boldsymbol{n}}^{(\mathrm{HL},i')} \end{bmatrix} \right) d\boldsymbol{z}_{\boldsymbol{n}}. \end{aligned} \tag{15}$$

By GSM, the latent chrominance and luminance coefficients $\mathcal{O}_{\boldsymbol{n}} | \boldsymbol{z}_{\boldsymbol{n}}$ are conditionally normal, with linear posterior mean

$$\mathbb{E}\left[\mathcal{O}_{\boldsymbol{n}} \Bigg| \begin{bmatrix} T_{\boldsymbol{n}}^{(\mathrm{LH},i')} \\ T_{\boldsymbol{n}}^{(\mathrm{HL},i')} \end{bmatrix}, \boldsymbol{z}_{\boldsymbol{n}} \right] = \Sigma_{\mathcal{O}T|\boldsymbol{z}} \Sigma_{T|\boldsymbol{z}}{}^{-1} \begin{bmatrix} T_{\boldsymbol{n}}^{(\mathrm{LH},i')} \\ T_{\boldsymbol{n}}^{(\mathrm{HL},i')} \end{bmatrix} \tag{16}$$

where

$$\Sigma_{\mathcal{O}T|\boldsymbol{z}} = \begin{bmatrix} z_{\boldsymbol{n}}^{\mathrm{LL}} \mathbf{\Sigma}^{\mathrm{LL}} & z_{\boldsymbol{n}}^{\mathrm{LL}} \mathbf{\Sigma}^{\mathrm{LL}} \\ z_{\boldsymbol{n}}^{\mathrm{LH}} \mathbf{\Sigma}^{\mathrm{LH}} & 0 \\ 0 & z_{\boldsymbol{n}}^{\mathrm{HL}} \mathbf{\Sigma}^{\mathrm{HL}} \end{bmatrix} \tag{17}$$

$$\Sigma_{T|\boldsymbol{z}} = \begin{bmatrix} z_{\boldsymbol{n}}^{\mathrm{LL}} \mathbf{\Sigma}^{\mathrm{LL}} + z_{\boldsymbol{n}}^{\mathrm{LH}} \mathbf{\Sigma}^{\mathrm{LH}} + \mathbf{\Lambda}_N & z_{\boldsymbol{n}}^{\mathrm{LL}} \mathbf{\Sigma}^{\mathrm{LL}} \\ z_{\boldsymbol{n}}^{\mathrm{LL}} \mathbf{\Sigma}^{\mathrm{LL}} & z_{\boldsymbol{n}}^{\mathrm{LH}} \mathbf{\Sigma}^{\mathrm{LL}} + z_{\boldsymbol{n}}^{\mathrm{HL}} \mathbf{\Sigma}^{\mathrm{HL}} + \mathbf{\Lambda}_N \end{bmatrix}. \tag{18}$$

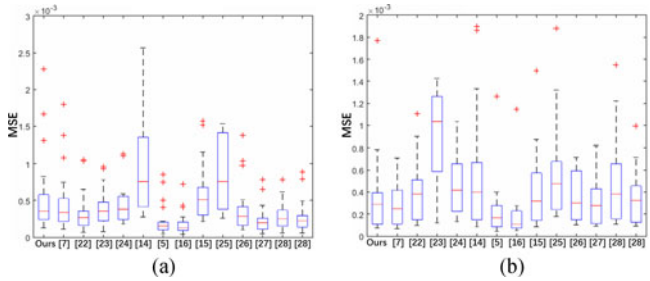

Fig. 2. Boxplot of MSE performance for the Kodak (24 images) and IMAX (18 images) datasets (red line = average MSE). Numbers on the x-axis correspond to references of the demosaicking methods compared. The last two shown in boxplot are the corresponding methods, with and without denoising part, respectively. (a) Kodak. (b) IMAX.

The density of the posterior mixture parameter $\boldsymbol{z}_{\boldsymbol{n}} | \boldsymbol{T}_{\boldsymbol{n}}$ can be computed by Bayes' theorem in a standard way

$$\begin{aligned} p\left(\boldsymbol{z}_{\boldsymbol{n}} \Bigg| \begin{bmatrix} T_{\boldsymbol{n}}^{(\mathrm{LH},i')} \\ T_{\boldsymbol{n}}^{(\mathrm{HL},i')} \end{bmatrix} \right) &= \frac{p\left(\begin{bmatrix} T_{\boldsymbol{n}}^{(\mathrm{LH},i')} \\ T_{\boldsymbol{n}}^{(\mathrm{HL},i')} \end{bmatrix} \Bigg| \boldsymbol{z}_{\boldsymbol{n}} = \boldsymbol{\alpha} \right) P(\boldsymbol{z}_{\boldsymbol{n}} = \boldsymbol{\alpha})}{\int\limits_{\mathbb{R}^3} p\left(\begin{bmatrix} T_{\boldsymbol{n}}^{(\mathrm{LH},i')} \\ T_{\boldsymbol{n}}^{(\mathrm{HL},i')} \end{bmatrix} \Bigg| \boldsymbol{z}_{\boldsymbol{n}} = \boldsymbol{\alpha} \right) P(\boldsymbol{z}_{\boldsymbol{n}} = \boldsymbol{\alpha})\, d\boldsymbol{\alpha}} \end{aligned} \tag{19}$$

where $P(\boldsymbol{z}_{\boldsymbol{n}} = \boldsymbol{\alpha})$ is the joint probability density function of $\boldsymbol{z}_{\boldsymbol{n}}$. We numerically compute (15) and (19) by integrating over the support of $\boldsymbol{z}_{\boldsymbol{n}}$ to estimate the chrominance and luminance wavelet coefficients $\widehat{V}_{\boldsymbol{n}}^{(\mathrm{LL},i')}$, $\widehat{U}_{\boldsymbol{n}}^{(\mathrm{LH},i')}$, and $\widehat{U}_{\boldsymbol{n}}^{(\mathrm{HL},i')}$. Additionally, $\widehat{U}_{\boldsymbol{n}}^{(\mathrm{LL},i')}$, $\widehat{U}_{\boldsymbol{n}}^{(\mathrm{HH},i')}$, and $\widehat{W}_{\boldsymbol{n}}^{(\mathrm{LL},i')}$ are reconstructed as follows[8]:

$$\begin{aligned} \widehat{U}_{\boldsymbol{n}}^{(\mathrm{LL},i')} &= \mathbb{E}[U_{\boldsymbol{n}}^{(\mathrm{LL},i')} | T_{\boldsymbol{n}}^{(\mathrm{LL},i')}] \\ \widehat{U}_{\boldsymbol{n}}^{(\mathrm{HH},i')} &= \mathbb{E}[U_{\boldsymbol{n}}^{(\mathrm{HH},i')} | T_{\boldsymbol{n}}^{(\mathrm{HH},i')}] \text{ for } J > \kappa \\ \widehat{W}_{\boldsymbol{n}}^{(\mathrm{LL},i')} &= \mathbb{E}[W_{\boldsymbol{n}}^{(\mathrm{LL},i')} | T_{\boldsymbol{n}}^{(\mathrm{HH},i')}] \text{ for } J \leqslant \kappa \end{aligned} \tag{20}$$

$\widehat{\boldsymbol{X}'}_{\boldsymbol{n}}$ is reconstructed via inverse wavelet transform.

Finally, we point out specific ways in which the proposed method addresses the differences between raw sensor data and demosaicking benchmarks in [5] and [6]. First, we overcome the issue that patch/window-based algorithms are sensitive to image resolution by using wavelet transforms, which are more robust to image resolution because of its multiscale decomposition. Second, since gamma correction in benchmark datasets influence the parameters and thresholds significantly, we learn $\mathbf{\Sigma}$ and probability density function $p(\boldsymbol{z}_{\boldsymbol{n}})$ directly from raw sensor data demosaicked by PSDD [7]. The use of PSDD for parameter training is justifiable because its artifacts occupy only a small portion of the output image. This technique also allows us to deduce image-specific parameters.

IV. Experiment Results

We conduct both the simulated data and real high-resolution sensor data experiments. The proposed algorithm was

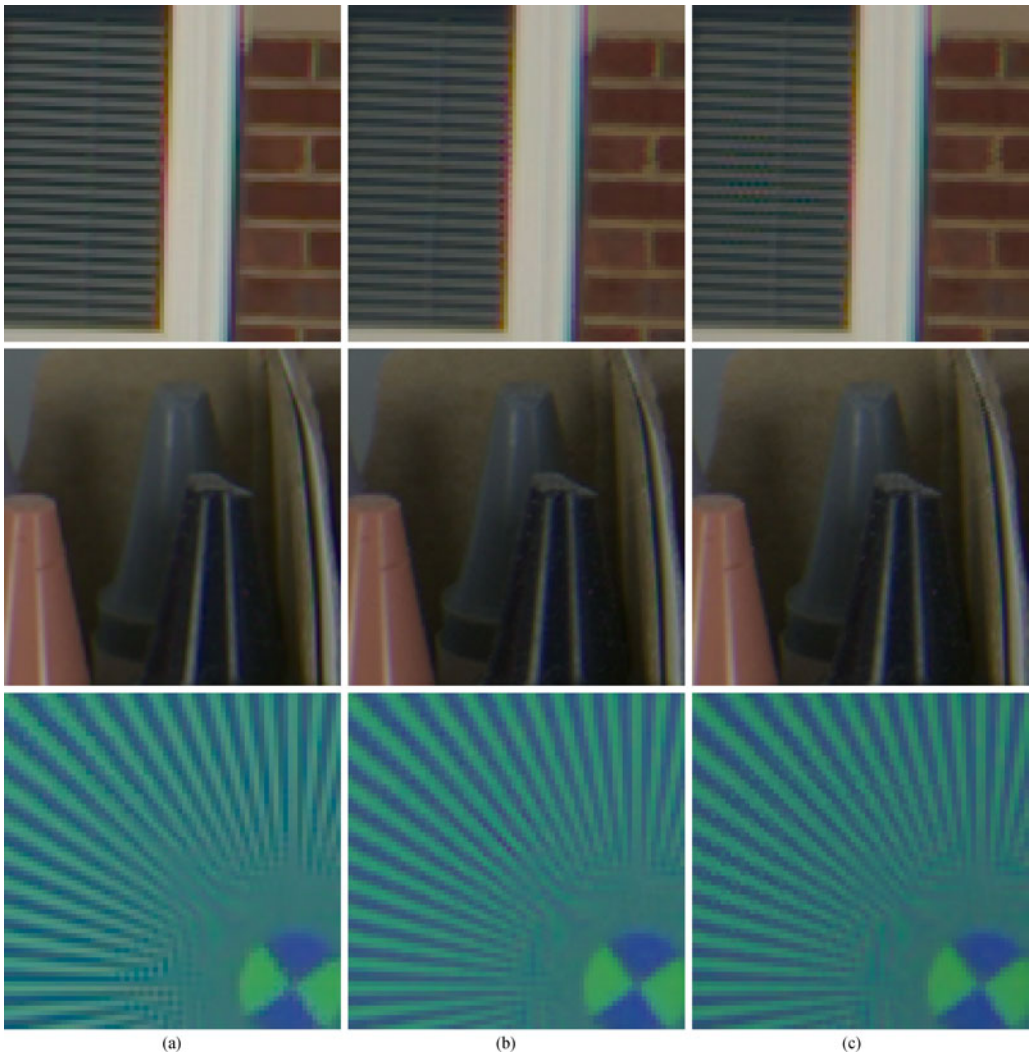

Fig. 3. Reconstructed results of various demosaicking algorithms. The results are cropped from the corresponding demosaicked outputs of D810FAR2I00100 (1st row), D810hSLI00100NR0 (2nd row), and D810hVFAI00100 (3rd row) (source: http://www.imaging-resource.com/). (a) Proposed. (b) [5]. (c) [16].

evaluated in terms of MSE performance for two widely used full-color image datasets—the Kodak (24 images, 768×512) [5] and IMAX (18 images, 500×500) [6] datasets. As stated earlier, we caution the readers that Kodak and IMAX images make poor approximation to raw sensor data. The full-color images were un gamma corrected and subsampled to form a Bayer CFA-patterned image. The MSE performance of demosaicking is shown in Fig. 2(a) and (b). Compared to the state-of-the-art demosaicking algorithms [5], [7], [14]–[16], [22]–[28], the proposed algorithm did not perform well.

However, consider demosaicking performance on real sensor data. We used raw sensor data from Nikon D810 and Sony α7RII (www.imaging-resource.com). These cameras lack optical low-pass filter, making the demosaicking most challenging. As shown by Fig. 3(a) and (c), and the supplemental materials, the proposed algorithm suppressed the zippering artifacts and improved the diagonal-image details, albeit slightly smoother and desaturated edges in the resolution chart image (bottom row). We contrast this to the demosaicking methods in [5] and [16], which were the best-performing methods according to the Kodak/IMAX datasets in Fig. 2. In actual sensor data that use real CFA colors at a much higher spatial resolution, methods in [5] and [16] suffered from zippering artifacts.

V. Conclusion

In this letter, we proposed a wavelet-GSM demosaicking algorithm. We significantly improved a demosaicking method called PSDD that fails when the wavelet coefficients are not sufficiently sparse. We replaced the sparsity assumption with a GSM and leveraged the spatial correlation of the wavelet coefficients. Although the MSE performance of the proposed demosaicking did not outperform the state-of-the-art methods based on Kodak and IMAX datasets, the proposed technique was superior at suppressing the zippering artifacts in real sensor images. We conclude that the proposed GSM-wavelet demosaicking is a better-suited choice for modern cameras. In future research, we plan to develop a raw sensor data-based benchmark for demosaicking performance.

Acknowledgement

The authors would like to thank the editorial staff at Imaging Resource for providing a written permission to reproduce their images.

REFERENCES

[1] B. E. Bayer, "Color Imaging array," U.S. Patent 3 971 065, Jul. 20, 1976.

[2] R. Ramanath, W. E. Snyder, G. L. Bilbro, and W. A. Sander, "Demosaicking methods for Bayer color arrays," *J. Electron. Imag.*, vol. 11, no. 3, pp. 306–315, 2002.

[3] X. Li, B. Gunturk, and L. Zhang, "Image demosaicing: A systematic survey," in *Proc. SPIE Int. Soc. Opt. Eng.*, 2008, pp. 68221J–68221J.

[4] D. Menon and G. Calvagno, "Color image demosaicking: An overview," *Signal Process., Image Commun.*, vol. 26, no. 8, pp. 518–533, 2011.

[5] D. Kiku, Y. Monno, M. Tanaka, and M. Okutomi, "Beyond color difference: Residual interpolation for color image demosaicking," *IEEE Trans. Image Process.*, vol. 25, no. 3, pp. 1288–1300, Mar. 2016.

[6] L. Zhang, X. Wu, A. Buades, and X. Li, "Color demosaicking by local directional interpolation and nonlocal adaptive thresholding," *J. Electron. Imag.*, vol. 20, no. 2, pp. 023016–023016, 2011.

[7] J. T. Korneliussen and K. Hirakawa, "Camera processing with chromatic aberration.," *IEEE Trans. Image Process.*, vol. 23, no. 10, pp. 4539–4552, Oct. 2014.

[8] J. Portilla, V. Strela, M. J. Wainwright, and E. P. Simoncelli, "Image denoising using scale mixtures of Gaussians in the wavelet domain," *IEEE Trans. Image Process.*, vol. 12, no. 11, pp. 1338–1351, Nov. 2003.

[9] D. R. Cok, "Signal processing method and apparatus for producing interpolated chrominance values in a sampled color image signal," U.S. Patent 4 642 678, Feb. 10, 1987.

[10] J. E. Adams, Jr. "Interactions between color plane interpolation and other image processing functions in electronic photography," in *Proc. IS&T/SPIE Symp. Electron. Imag., Sci. Technol.*, 1995, pp. 144–151.

[11] K. Hirakawa, X.-L. Meng, and P. J. Wolfe, "A framework for wavelet-based analysis and processing of color filter array images with applications to denoising and demosaicing," in *Proc. 2007 IEEE Int. Conf. Acoust., Speech Signal Process.*, 2007, vol. 1, pp. I-597–I-600.

[12] E. Dubois, "Frequency-domain methods for demosaicking of Bayer-sampled color images," *IEEE Signal Process. Lett.*, vol. 12, no. 12, pp. 847–850, Dec. 2005.

[13] K. Hirakawa and P. J. Wolfe, "Spatio-spectral color filter array design for enhanced image fidelity," in *Proc. 2007 IEEE Int. Conf. Image Process.*, 2007, vol. 2, pp. II-81–II-84.

[14] D. Kiku, Y. Monno, M. Tanaka, and M. Okutomi, "Residual interpolation for color image demosaicking," in *Proc. 2013 IEEE Int. Conf. Image Process.*, 2013, pp. 2304–2308.

[15] D. Kiku, Y. Monno, M. Tanaka, and M. Okutomi, "Minimized-Laplacian residual interpolation for color image demosaicking," *Proc. SPIE*, vol. 9023, pp. 2304–2308, 2014.

[16] Y. Monno, D. Kiku, M. Tanaka, and M. Okutomi, "Adaptive residual interpolation for color image demosaicking," in *Proc. 2015 IEEE Int. Conf. Image Process.*, pp. 3861–3865.

[17] N. Zhang and X. Wu, "Lossless compression of color mosaic images," *IEEE Trans. Image Process.*, vol. 15, no. 6, pp. 1379–1388, Jun. 2006.

[18] K. Hirakawa and P. J. Wolfe, "Rewiring filterbanks for local Fourier analysis: Theory and practice," *IEEE Trans. Inf. Theory*, vol. 57, no. 8, pp. 5360–5374, Aug. 2011.

[19] D. Alleysson, S. Susstrunk, and J. Hérault, "Linear demosaicing inspired by the human visual system," *IEEE Trans. Image Process.*, vol. 14, no. 4, pp. 439–449, Apr. 2005.

[20] J. W. Glotzbach, R. W. Schafer, and K. Illgner, "A method of color filter array interpolation with alias cancellation properties," in *Proc. IEEE 2001 Int. Conf. Image Process.*, 2001, vol. 1, pp. 141–144.

[21] B. K. Gunturk, J. Glotzbach, Y. Altunbasak, R. W. Schafer, and R. M. Mersereau, "Demosaicking: Color filter array interpolation," *IEEE Signal Process. Mag.*, vol. 22, no. 1, pp. 44–54, Jan. 2005.

[22] K. Hirakawa and T. W. Parks, "Adaptive homogeneity-directed demosaicing algorithm," *IEEE Trans. Image Process.*, vol. 14, no. 3, pp. 360–369, Mar. 2005.

[23] L. Zhang and X. Wu, "Color demosaicking via directional linear minimum mean square-error estimation," *IEEE Trans. Image Process.*, vol. 14, no. 12, pp. 2167–2178, Dec. 2005.

[24] Y. M. Lu, M. Karzand, and M. Vetterli, "Demosaicking by alternating projections: Theory and fast one-step implementation," *IEEE Trans. Image Process.*, vol. 19, no. 8, pp. 2085–2098, Aug. 2010.

[25] S. P. Jaiswal, O. C. Au, V. Jakhetiya, Y. Yuan, and H. Yang, "Exploitation of intercolor correlation for color image demosaicking," in *Proc. 2014 IEEE Int. Conf. Image Process.*, 2014, pp. 1812–1816.

[26] B. Leung, G. Jeon, and E. Dubois, "Least-squares luma–chroma demultiplexing algorithm for bayer demosaicking," *IEEE Trans. Image Process.*, vol. 20, no. 7, pp. 1885–1894, Jul. 2011.

[27] M. H. Davis *et al.*, "Dissociating speech perception and comprehension at reduced levels of awareness," *Proc. Nat. Acad. Sci. U.S.A.*, vol. 104, no. 41, pp. 16032–16037, 2007.

[28] D. Paliy, V. Katkovnik, R. Bilcu, S. Alenius, and K. Egiazarian, "Spatially adaptive color filter array interpolation for noiseless and noisy data," *Int. J. Imag. Syst. Technol.*, vol. 17, no. 3, pp. 105–122, 2007.